Statistical analysis of correlated resonance phenomena in two systems: $^{28}Si+^{20}Ne$ and $^{24}Mg+^{20}Ne$

S. P. Barrow, R. W. Zurmühle, D. R. Benton, Y. Miao, Q. Li,* P. H. Kutt, Z. Liu, C. Lee,† N. G. Wimer, and J. T. Murgatroyd*

Department of Physics and Astronomy, University of Pennsylvania, Philadelphia, Pennsylvania 19104

(Received 16 June 1995)

A differentially pumped windowless ^{20}Ne gas target was used to measure angle averaged excitation functions for binary decay of the $^{28}Si+^{20}Ne$ reaction into low-lying states of $^{28}Si+^{20}Ne$, $^{24}Mg+^{24}Mg$, and $^{32}S+^{16}O$, and for binary decay of the $^{24}Mg+^{20}Ne$ reaction into low-lying states of $^{24}Mg+^{20}Ne$ and $^{28}Si+^{16}O$. The $^{28}Si+^{20}Ne$ measurements span the region of excitation energy in ^{48}Cr from 50.6 to 67.7 MeV (^{28}Si beam energies from 87.2 to 128.2 MeV). The reaction $^{24}Mg+^{20}Ne$ was investigated over a region in ^{44}Ti from 48.75 to 71.0 MeV (^{24}Mg beam energies from 70.8 to 119.75 MeV). Angular distribution measurements were made for $^{20}Ne(^{28}Si,^{24}Mg)^{24}Mg$ at excitation energy=56.22 MeV and for $^{20}Ne(^{24}Mg,^{16}O)^{28}Si$ at excitation energy=53.02 and 57.75 MeV. Both systems display evidence of statistically significant correlated resonance phenomena, but the resonances are dominated by spins comparable to the grazing angular momenta of the respective entrance channels, and are not analogs of the molecular configurations that dominate the $^{24}Mg(^{24}Mg,^{24}Mg^*)^{24}Mg^*$ reactions.

PACS number(s): 25.70.Ef, 25.70.Hi

I. INTRODUCTION

One of the most striking results to emerge from studies of the elastic and inelastic scattering of *s-d* shell nuclei are the presence of pronounced and highly correlated resonances in some of these systems. The first evidence of resonance behavior in the binary decay of a reaction between two *s-d* shell nuclei for center of mass energies well above the Coulomb barrier was in the $^{28}Si+^{28}Si$ system [1–4], in which intermediate width ($\Gamma\sim150$ keV) and wide ($\Gamma\sim$few MeV) structures were observed. Some of the intermediate width structures are common to several of the decay channels into low-lying excited states in ^{28}Si, including the elastic channel. The on-resonance elastic scattering angular distribution measurements for center of mass angles near 90° are dominated by partial waves comparable to the grazing angular momenta of $^{28}Si+^{28}Si$ calculated by optical model potentials. Similar resonances are found in the $^{28}Si+^{24}Mg$ system [5].

The most strongly correlated structures found to date have been observed in the $^{24}Mg+^{24}Mg$ system [6,7]. Not only are they the most strongly correlated, but in this system the spins of the resonances are four units of angular momentum larger than grazing values based on optical model calculations for two spherical ^{24}Mg nuclei [8,9]. A subsequent study of the reaction $^{24}Mg(^{24}Mg,^{20}Ne^*)^{28}Si^*$ [10] surveyed a 3 MeV wide region of excitation energy, and gives some evidence for decay into low-lying excitations of $^{28}Si+^{20}Ne$ from the structures seen in the elastic and inelastic scattering of $^{24}Mg+^{24}Mg$. For each resonance studied, these two binary decay mass partitions account for approximately 20% of the total decay strength of an isolated Breit-Wigner resonance [10], with the $^{24}Mg+^{24}Mg$ channel at least 5 times stronger than the $^{28}Si+^{20}Ne$ channel. In the current work a much more detailed study of the $^{28}Si+^{20}Ne$ reaction is presented to determine if such a high level of correlation is typical for the $^{28}Si+^{20}Ne$ and $^{24}Mg+^{24}Mg$ mass partitions. Evidence of correlated structure between several mass partitions is not limited to composite nuclei with $A=48$, as, for example, correlated structure between $^{28}Si(^{28}Si,^{28}Si^*)^{28}Si^*$ and $^{16}O(^{40}Ca,^{28}Si^*)^{28}Si^*$ [11] has also been reported.

Of course it is impossible to fully understand these resonances without understanding the reasons other systems do not manifest similar phenomena. Previous investigations have focused on $^{28}Si+^{29}Si$, $^{28}Si+^{30}Si$, and $^{30}Si+^{30}Si$ [12], and no evidence of correlated resonance structures was found. A comparison of the neutron separation energies of the composite nuclei [9] reveals that all those systems which display resonance behavior have large neutron separation energies, and that this is a property unique to some of the even N, even Z, $N=Z$ so-called "alpha particle" nuclei such as ^{48}Cr and ^{44}Ti. It seems likely that for nuclei with small neutron separation energies, high spin resonances will decay by neutron evaporation, and the branching ratios into fission channels will be unobserveably small, although this has not been verified experimentally.

Studies done on the alpha particle nuclei systems $^{40}Ca+^{40}Ca$ [12], $^{32}S+^{32}S$ [13], and $^{20}Ne+^{20}Ne$ [14] also did not show any correlated resonances. The results for the $^{20}Ne+^{20}Ne$ system are particularly surprising, as Beck *et al.* [15] used the number of open channels to study the observation of resonances for systems ranging in size from $^{16}O+^{16}O$ to $^{32}S+^{32}S$, and concluded that $^{20}Ne+^{20}Ne$ is even more favorable than the $^{24}Mg+^{24}Mg$ system for manifesting pronounced resonances.

Reaction models which reproduce the gross structures seen in lighter systems, for example, $^{12}C+^{12}C$ [16,17] and

*Present address: Wayne State University, Detroit, Michigan 48202.

†Present address: Florida State University, Tallahassee, Florida 32306.

$^{16}O+^{16}O$ [18], such as the band crossing model [19,20], the double resonance model [21–26], a coupled channels calculation [27], the barrier top model [28], the doorway state model [29], and the Austin-Blair model [30], are unable to generate the narrow correlated structures that dominate the $^{24}Mg+^{24}Mg$ reaction. The $^{24}Mg+^{24}Mg$ excitation functions appear to be dominated by the population of highly excited compound states in ^{48}Cr, and this experimental result has prompted much theoretical work on the properties of *s-d* shell nuclei at high spin and high excitation energy. These nuclear structure models of ^{48}Cr are as follows: a 16-particle–8-hole (16p-8h) excitation in the Hartree-Fock framework [31], a two-center shell model with a neck degree of freedom [32], a molecular model which considers collective motions in terms of a rotating dinuclear system [33], an alpha cluster model which uses a Brink-Boeker nucleon-nucleon interaction [34], a combination of the molecular and the two-center shell models [35,36], and a rotating liquid drop model [8,9].

The Hartree-Fock model [31] reproduces fairly well the spin versus excitation energy dependence of the resonances in the $^{28}Si+^{28}Si$ system, but it considerably overestimates the energy spacing between adjacent resonances in the $^{24}Mg+^{24}Mg$ system, as well as the excitation energy in ^{48}Cr for each of the observed spins, which suggests that these calculated states are different from the observed molecular configurations, and that the resonances in $^{24}Mg+^{24}Mg$ have larger deformations than the model states. The molecular model with macroscopic degrees of freedom [33] predicts a local minimum in the potential energy surface for pole-to-pole alignment of the ^{24}Mg nuclei. This configuration corresponds to the largest possible moment of inertia for two touching ^{24}Mg nuclei, and on that basis is a candidate for being the yrast states in this region of high excitation energy. This model is also used to calculate the partial widths of the molecular configurations for decay into low-lying excitations in the $^{24}Mg+^{24}Mg$ mass partition, and predicts a large parentage of the elastic and low-lying inelastic channels for some of the configurations, in qualitative agreement with the experimental partial widths. The molecular model can easily account for the fragmentation of a single spin into several resonances with the introduction of vibrational modes of excitation to the collective motion. In fact, it predicts the existence of many more quasimolecular configurations than are observed experimentally, but many of the predicted states have widths on the order of a few eV, and therefore would be unobservable in resonance measurements. Similar calculations of the partial widths for high spin configurations in ^{48}Cr have been done using the two-center shell framework [35], and here too the agreement with the measured partial widths for symmetric binary decay is very good. Not much theoretical work has been done on the partial widths of the binary decay of the molecular resonances into nonidentical nuclei such as decay from the high spin configurations in ^{48}Cr into $^{28}Si+^{20}Ne$. The alpha cluster model [34] uses the Bloch-Brink cranked cluster formalism to study highly deformed rotational bands with a 3-to-1 axis ratio for several nuclei that are "doubly magic" at large deformation, such as ^{12}C, ^{36}Ar, and ^{48}Cr. For ^{48}Cr, these hyperdeformed states resemble a chain of three ^{16}O nuclei, which suggests that this rotational band would have substantial branching ratios for decay into $^{16}O+^{32}S$ or $^{16}O+^{16}O+^{16}O$. The rotating liquid drop model [8,9] was used to calculate the fission barriers, fission paths, and equilibrium shapes for high spin states in ^{48}Cr.

The models are consistent in that they suggest the prolate deformation of the ground state of ^{24}Mg is crucial for the population of these high spin molecular configurations, as the shapes of the molecular configurations in ^{48}Cr resemble two ^{24}Mg nuclei aligned pole to pole along their major axis. This supports the speculation that the phenomena that dominates the $^{24}Mg+^{24}Mg$ system are "shape matching" resonances between the $^{24}Mg+^{24}Mg$ entrance channel and individual high spin excited states in ^{48}Cr. This discussion indicates the $^{24}Mg+^{20}Ne$ system might be a good candidate for manifesting resonance phenomena, as this reaction also studies two alpha particle nuclei with large ground state prolate deformation. In addition, the $^{24}Mg+^{20}Ne$ system is interesting since it is a mass asymmetric entrance channel, which could provide insight about the importance of the mass symmetry on the shape matching. In this work we present a major study of the $^{24}Mg+^{20}Ne$ system.

The cross sections for $^{28}Si+^{20}Ne$ were measured over a region of excitation energy in ^{48}Cr from 50.6 to 67.7 MeV (c.m. energies from 36.3 to 53.4 MeV), which spans the region from 1.5 to 2.1 times the Coulomb barrier for two spherical mass-24 nuclei. The reaction $^{24}Mg+^{20}Ne$ was investigated over a region of excitation energy in ^{44}Ti from 48.75 to 71.0 MeV (c.m. energies from 32.2 to 54.4 MeV), which spans the region from 1.6 to 2.4 times the Coulomb barrier for a spherical mass-24 and mass-20 nucleus. Statistical analysis techniques will be used to quantify the degree of correlated resonance structure in the $^{28}Si+^{20}Ne$ and $^{24}Mg+^{20}Ne$ systems. Angular distributions were measured for each reaction, and spin assignments from the angular distributions are used to determine the spins of the resonances and their relation to the grazing angular momenta of the entrance and exit channels. Both experiments used the differentially pumped windowless ^{20}Ne gas target that was recently built at the University of Pennsylvania Tandem Accelerator Laboratory.

II. EXPERIMENTAL METHOD

The ^{28}Si and ^{24}Mg beams were provided by the University of Pennsylvania Tandem Accelerator at the University of Pennsylvania, Philadelphia, Pennsylvania, and the Wright Nuclear Structure Laboratory at Yale University, New Haven, Connecticut. The Wright Nuclear Structure Laboratory accelerator was used to measure the cross sections for beam energies larger than those easily produced by the University of Pennsylvania Tandem Accelerator. Measurements over a small energy region were carried out at both facilities to obtain an accurate relative calibration of the two accelerators, and an absolute calibration [37] of the University of Pennsylvania Accelerator was done using an 1 keV wide $J^{\pi}=\frac{3}{2}^{-}$ resonance in the $^{12}C(p,\gamma)$ reaction. The calibrations revealed that the actual University of Pennsylvania Tandem beam energies were 0.563% higher than the nominal value, while the Yale energies were too high by 2.47%. The corrected beam energies were used for playback of the data. For both the ^{24}Mg and ^{28}Si beams the excitation functions were

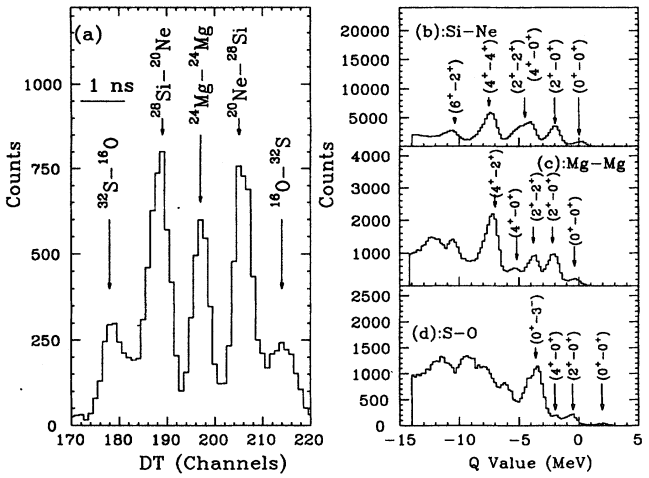

FIG. 1. ^{28}Si+^{20}Ne mass partitions and Q spectra.

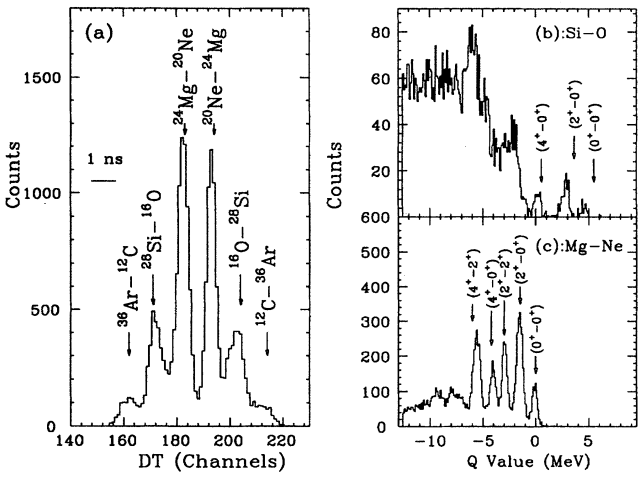

FIG. 2. ^{24}Mg+^{20}Ne mass partitions and Q spectra.

measured in 200 keV steps in the laboratory system, which translates to 90.9 keV and 83.3 keV in the center of mass system, respectively. Typical runs took from 1 to 2 h for each beam energy. The angular distribution runs were much longer, 1.5 to 2 days each.

The ^{20}Ne gas target used in this work has been described elsewhere [14,37], and a detailed discussion of the target will be presented in a future publication. The thickness of the target was 11 μg/cm^2, which corresponds to an energy loss of roughly 50 keV for these beams and beam energies. Two (2.0 cm)×(4.0 cm) heavy ion surface barrier detectors were positioned on either side of the beam at ±40°, and we studied coincidence events in which each detector was struck by one decay fragment. From the time of flight difference of the two decay fragments, as well as their energies, we were able to reconstruct the masses of the two fragments, which mass struck which detector, the Q value of the reaction, and for the angular distribution measurements, the value of the center of mass angle $\theta_{\text{c.m.}}$. The mass partitions that dominate each reaction, as well as the Q spectra for the strongest mass partitions, are shown in Figs. 1 and 2 for the ^{28}Si+^{20}Ne and ^{24}Mg+^{20}Ne reactions, respectively. Only events in which the sum of the two energy signals corresponded to a Q value greater than approximately −30 MeV were included in the time of flight mass partition figures, where DT is the calculated time of flight difference of the two fragments. This restriction excluded many-body decays in which only two of the fragments struck the detectors. The resolution of the time of flight difference is typically 600 ps full width at half maximum (FWHM), and the energy resolution of the elastic peaks is typically 500 keV (FWHM). The peaks labeled by the vertical arrows in Figs. 1(b)–1(d) and Figs. 2(b) and 2(c) are the focus of the statistical analysis of correlated resonance phenonema. The counts in these peaks were summed, and after proper normalization, plotted as a function of excitation energy in the composite nucleus. The absolute cross sections for each measurement were calculated by recording the integrated charge of the beam in a Faraday cup postioned downstream of the ^{20}Ne target area, and by monitoring the pressure of the ^{20}Ne gas in the target region with a pressure transducer. There is a 500 μg/cm^2 nickel foil downstream of the ^{20}Ne target area, which ensures the vast majority of beam nuclei will be fully stripped of orbiting electrons before entering the Faraday cup. The solid angle of the recoil coincidence for each mass partition was calculated using a Monte Carlo technique [37], as the spatial extent of the gas target over 1 cm in length makes it difficult to calculate the solid angle directly. The simulated solid angles reflect the differences in the detection efficiencies for these two-body decay channels due to the fixed detector geometry.

III. ANALYSIS TECHNIQUES

It has been understood for some time that the presence of structures in an excitation function does not prove that a compound nuclear state has been populated. Ericson showed [38] that in the region of excitation energy in the compound nucleus for which there are many overlapping levels (such as in the current work), the so-called statistical fluctuations in the cross sections can result in structures in the excitation functions, but that different structures are present in each exit channel.

The statistical analysis in the current work is based on the energy-dependent function $Y_K(E)$ defined by

$$Y_K(E)=\frac{\sigma_K(E)}{\langle\sigma_K(E)\rangle}, \tag{1}$$

where $\sigma_K(E)$ is the cross section for the Kth reaction at center of mass energy E, and $\langle\sigma_K(E)\rangle$ is a local square average over an energy region Δ from $E_i=E-\Delta/2$ to $E_i=E+\Delta/2$ of the cross section $\sigma_K(E_i)$. The frequency distribution $P(Y_K)$ of $Y_K(E)$ [39–41] is given by

$$P(Y_K)=\frac{N_K}{1-Y_{Dk}}\left[\frac{Y_K}{Y_{Dk}}\right]^{(N_K-1)/2}\exp\left[-\frac{N_K(Y_K+Y_{Dk})}{(1-Y_{Dk})}\right]\times I_{N_K-1}\left[\frac{2N_k(Y_KY_{Dk})^{1/2}}{(1-Y_{Dk})}\right]. \tag{2}$$

The expression for $P(Y_K)$ in Eq. (2) is a complicated function of N_K, the number of independent channels in the reac-

tion, Y_{Dk}, the nonfluctuating direct component to the average cross section, and I_N, the modified Bessel function of order N. The frequency distribution will vary from reaction to reaction due to the dependence of $P(Y_K)$ on the values of N_K, Y_{Dk}, and I_N, which are not universal quantities, but specific parametrizations for each reaction. A common technique to study simultaneously the resonance behavior of many reactions is to use a frequency distribution function $P(D_i)$, where the deviation function $D_i(E)$ is defined as

$$D_i(E)=\frac{Y_i(E)-\langle\langle Y_i\rangle\rangle}{\sqrt{\langle\langle Y_i^2\rangle\rangle-\langle\langle Y_i\rangle\rangle^2}}, \tag{3}$$

and $\langle\langle\ \rangle\rangle$ denotes an average over the entire energy range of the excitation function. This is a useful definition of the deviation function since the frequency distribution of $D_i(E)$ is nearly Gaussian in shape with a mean and standard deviation of 0 and 1, respectively, for all reactions regardless of the values of N_K, Y_{Dk}, and I_N in $P(Y_K)$. The discrepancies from a Gaussian distribution [4] are significant only for very large positive and negative values of $D_i(E)$.

The summed deviation function is defined by

$$\mathscr{D}(E)=\frac{1}{N}\sum_{i=1}^{N} D_i(E), \tag{4}$$

where N is the number of excitation functions included in the summation. The probabilty distribution $P(\mathscr{D})$ for statistical fluctuations has been shown [4] to be very close to that obtained from treating the D_i's as independent functions; the mean μ of $P(\mathscr{D})$ is then 0 and the variance σ^2 is given by

$$\sigma^2[P(\mathscr{D})]=\frac{1}{N^2}\sum_{i=1}^{N}\sigma^2_{P(D)}=\frac{1}{N}. \tag{5}$$

To isolate instances in which several of the reactions have concurrent positive values of $\mathscr{D}(E)$, the cross-correlation function $C(E)$ is used, which is defined as

$$C(E)=\frac{2}{N(N-1)}\sum_{i>j=1}^{N} D_i(E)D_j(E). \tag{6}$$

The cross-correlation function sums over all pairs of products of the individual deviation functions. By combining the results of $\mathscr{D}(E)$ and $C(E)$, it is possible to isolate the instances in which all or many of the exit channels have resonances in their excitation functions, as these are the only cases for which both $\mathscr{D}(E)$ and $C(E)$ will have large positive values.

Calculating the probability density $P(C)$ is not trivial, as $C(E)$ is a sum of products of pairs. The terms in the summation of Eq. (6) cannot be treated separately as was done for $\mathscr{D}(E)$. However, the probability densities for $D_i(E)$ are known, and therefore $P(C)$ can be estimated using the Monte Carlo technique. Much work has already appeared in the literature [4,10,11] that has performed Monte Carlo calculations, and a comparison of those results makes it possible to derive a functional representation of the variance of $C(E)$ on the number of terms n included in the summation. Based on these simulations the variance of the statistical fluctuations in $C(E)$ can be expressed to within 1% accuracy by

$$\sigma^2[P(C)]=\frac{1}{n}, \tag{7}$$

where n is the number of terms in the summation in Eq. (6). For a cross-correlation analysis that considers all possible pairs of N excitation functions, the functional form of the standard deviation of the frequency distribution of $C(E)$ using Eq. (7) can be expressed as a function of N by

$$\sigma^2[P(C)]=\frac{1}{n}=\frac{2}{N(N-1)}. \tag{8}$$

The Monte Carlo simulations only consider values of n ranging from $n=3$ to 10, and therefore this functional representation should only be considered valid for the same interval. In this work we use the approximation that the frequency distribution $P(C)$ is a Gaussian distribution with a mean $\mu=0.0$ and a standard deviation given by Eq. (8).

The above discussion considers the probablity distribution $P(C)$ which is produced by the probablity distributions $P(D)$ of the deviation functions in Eq. (6). There is also an experimental uncertainty for both $C(E)$ and $D(E)$ which is due to the finite range of data (the uncertainty related to the sample size) [42]. This uncertainty is ignored in the current work.

The autocorrelation function [7] is used to determine the appropriate averaging interval Δ for the excitation functions of interest. The autocorrelation function $R(\epsilon=0)$ for a given reaction channel $\sigma_K(E)$ is defined by

$$R(0)=\frac{\langle\langle Y_K^2(E)\rangle\rangle}{\langle\langle Y_K(E)\rangle\rangle^2}-1. \tag{9}$$

This expression uses the definition for $Y_K(E)$ given in Eq. (1), and the $\langle\langle\ \rangle\rangle$ denote an averaging over the entire energy range of the excitation function. The standard convention is to plot $R(0)$ as a function of the averaging interval Δ, and use the smallest value of Δ at which $R(0)$ begins to level off and forms a plateau. This assumes that there are two scales of widths in the excitation function Γ_{fine} and Γ_{gross}. The plateau region corresponds to an averaging interval Δ such that $\Gamma_{\text{fine}}\ll\Delta\ll\Gamma_{\text{gross}}$.

IV. RESULTS AND ANALYSIS FOR ^{28}Si+^{20}Ne

Figure 3 shows the autocorrelation function $R(0)$ as a function of the averaging interval Δ for the mutual ground state exit channel of each mass partition. The autocorrelation functions are similar and all three have reached a plateau for values of Δ of 1.5 MeV. The ^{24}Mg+^{24}Mg and ^{28}Si+^{20}Ne functions actually level off at smaller values of Δ, around 1.2 MeV, while the ^{32}S+^{16}O function levels off more gradually. However, for $\Delta=1.2$ MeV the ^{32}S+^{16}O autocorrelation function is very near its plateau value, so $\Delta=1.2$ MeV will be used as the averaging interval for all three mass partitions. The results of the statistical analysis are not very sensitive to the specific value of the averaging interval, as long as it is

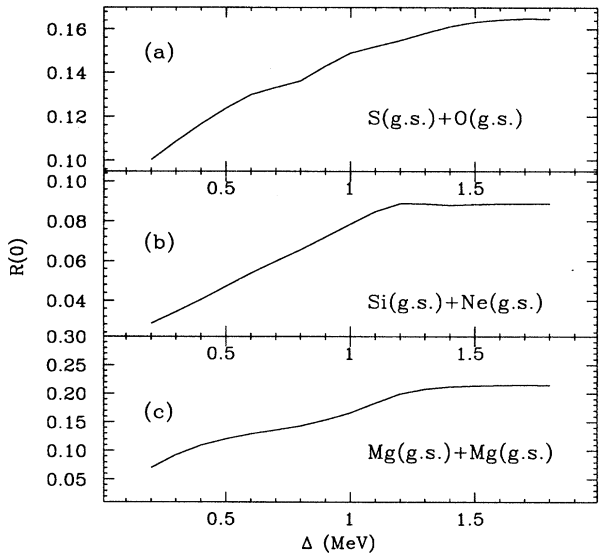

FIG. 3. Autocorrelation functions for the ground-state–ground-state exit channel of each mass partition studied in the ^{28}Si+^{20}Ne system.

near or within the plateau region. The excitation functions used for this analysis are plotted later in this section.

The excitation functions for the ^{24}Mg+^{24}Mg mass partition are plotted in Fig. 4. These reactions share the same exit channels as were studied in ^{24}Mg(^{24}Mg,^{24}Mg*)^{24}Mg* [6], and therefore are the most likely ones to exhibit resonance behavior at the energies of the molecular configurations. It is immediately apparent that there is a great deal of structure in all five excitation functions. However, in contrast to the results for ^{24}Mg(^{24}Mg,^{24}Mg*)^{24}Mg* [6], there are no instances of several excitation functions displaying identical resonance

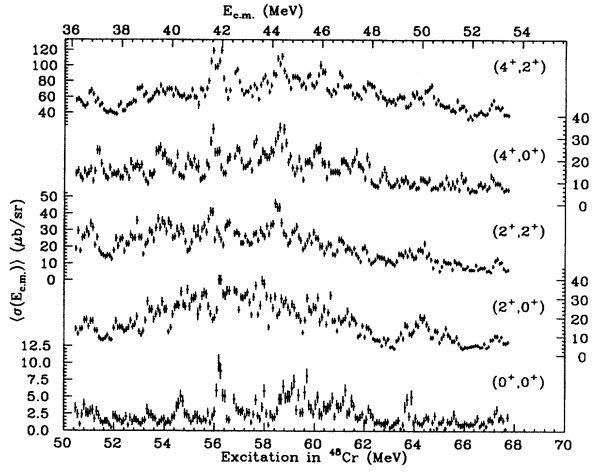

FIG. 4. Excitation functions for the ^{24}Mg+^{24}Mg mass partition exit channels. The $(0^+,0^+)$ excitation function is averaged over the angle range $68° \leq \theta_{c.m.} \leq 112°$. The x axis is labeled with the excitation energy in ^{48}Cr at the bottom and with the entrance channel center of mass energy on top.

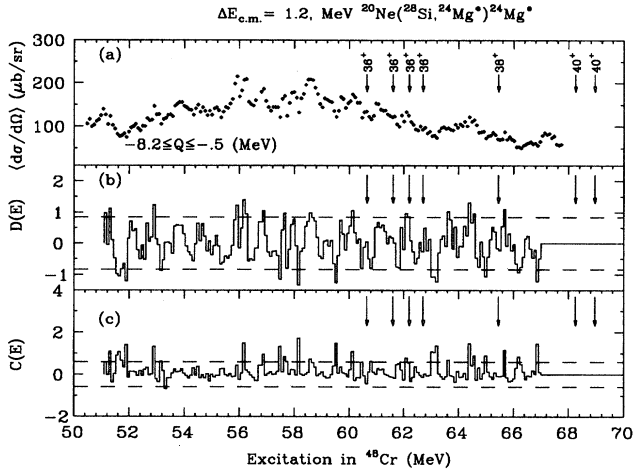

FIG. 5. (a) Sum of the excitation functions shown in Fig. 4, (b) summed deviation function, (c) cross-correlation function. The vertical arrows indicate the centroid energies for the molecular configurations [6], and the spin assignments are also listed.

behavior, and the resonances in these excitation functions are qualitatively more similar to the behavior observed in the ^{28}Si+^{28}Si [4] and ^{28}Si+^{24}Mg [5] systems. The widths of the structures in the current work are similar to those seen in ^{24}Mg(^{24}Mg,^{24}Mg*)^{24}Mg* [6], ranging from a few hundred keV, such as the peak in the $(0^+,0^+)$ channel centered at excitation energy=56.2 MeV, up to roughly 1 MeV, such as the peak centered at 58.25 MeV in the $(2^+,2^+)$ channel.

The cross-correlation and summed deviation functions, using all possible pairs of the five excitation functions and all five excitation functions, respectively, are shown in Fig. 5, along with the excitation energy-dependent sum of the cross sections of the five exit channels. The dashed horizontal lines represent the 95% confidence limits for statistical fluctuations using Gaussian distributions. There are some instances of statistically significant correlated resonance structure, such as at 56.2 MeV, in which both the cross-correlation and summed deviation functions exceed the 95% confidence limits, and the summed excitation functions cross section has a peak. The vertical arrows in Fig. 5 denote the centroid energies of the molecular configurations observed in ^{24}Mg(^{24}Mg,^{24}Mg*)^{24}Mg* [6]; the spin assignments [8] are indicated in Fig. 5(a). Although there are a few instances of correlated resonances at approximately the same energies as the molecular resonances, such as at 62.1 and 65.65 MeV, the correlations are not as strong as they were for the elastic and inelastic scattering of ^{24}Mg+^{24}Mg [7], and decay from the molecular resonances in ^{48}Cr is not the dominant reaction mechanism for the ^{20}Ne(^{28}Si,^{24}Mg*)^{24}Mg* reactions. Except for the $(0^+,0^+)$ and $(2^+,2^+)$ exit channels, odd partial waves are not forbidden in these reactions, and it is possible that their presence is obscuring decay from the molecular configurations in ^{48}Cr. However, even if this were the case, the branching ratios would still be small since they are presently unobservable. The fact the ^{28}Si+^{20}Ne and ^{24}Mg + ^{24}Mg entrance channels are angular momentum matched [37] suggests that microscopic considerations play an impor-

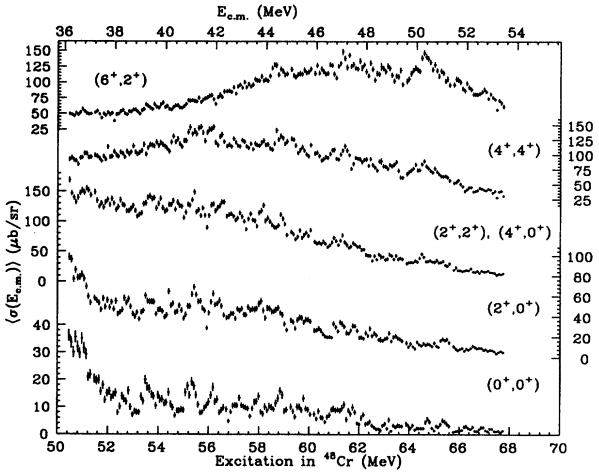

FIG. 6. Excitation functions for the ^{28}Si+^{20}Ne mass partition exit channels. The $(0^+,0^+)$ excitation function is averaged over the angle range $72°\leq\theta_{c.m.}\leq104°$. The x axis is labeled with the excitation energy in ^{48}Cr at the bottom and with the entrance channel center of mass energy on top.

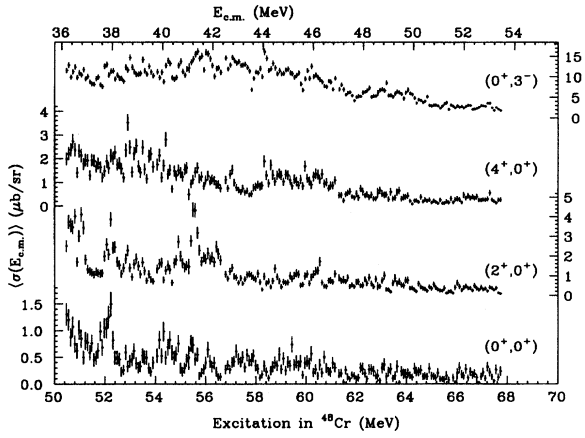

FIG. 8. Excitation functions for the ^{32}S+^{16}O mass partition. The $(0^+,0^+)$ excitation function is averaged over the angle range $50°\leq\theta_{c.m.}\leq113°$. The x axis is labeled with the excitation energy in ^{48}Cr at the bottom and with the entrance channel center of mass energy on top.

tant role, and that strong shape matching between the ^{24}Mg+^{24}Mg channel and the molecular configurations greatly increase the branching ratios for decay into low-lying excited states of ^{24}Mg+^{24}Mg.

The excitation functions for the ^{28}Si+^{20}Ne mass partition are shown in Fig. 6. The structures in this mass partition have widths similar to those seen in Fig. 4. The functional analysis for these five excitation functions is shown in Fig. 7. Except for a correlated resonance at 56.2 MeV, the two mass partitions do not have resonance structures in common. There is no evidence of resonance structures in the ^{28}Si+^{20}Ne mass partition at the energies of the molecular configurations (the value of the positive cross-correlation function at excitation energy=60.75 MeV corresponds to a minimum in the summed excitation function).

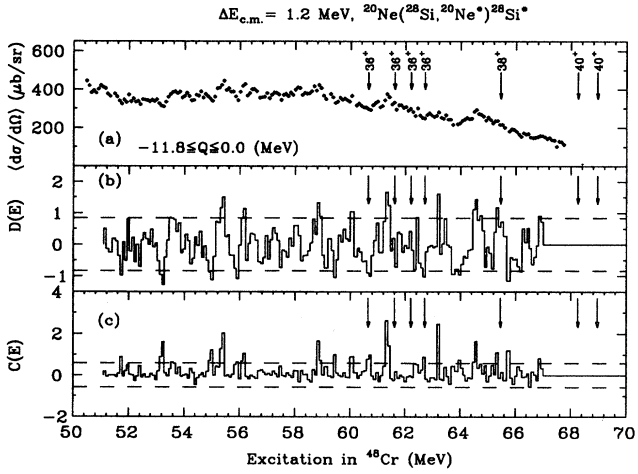

FIG. 7. (a) Sum of the excitation functions shown in Fig. 6, (b) summed deviation function, (c) cross-correlation function. The vertical arrows indicate the centroid energies for the molecular configurations [6], and the spin assignments are also listed.

The excitation functions for the ^{32}S+^{16}O mass partition are shown in Fig. 8. The most pronounced structures are present in the lower halves of the excitation functions, below the energies of the known molecular configurations. The cross sections for this mass partition are very small: typically 1/30th the strength of the ^{28}Si+^{20}Ne exit channels, and 1/6th the strength of the ^{24}Mg+^{24}Mg exit channels. There is a resonance in the $(0^+,0^+)$ channel in the vicinity of 56.2 MeV, so all three mass partitions manifest resonance activity at this energy, although the structure in the ^{32}S+^{16}O mass partition is centered at a slightly lower energy and is wider than the structures in the other two mass partitions, and therefore it is not certain that this decay is from the same resonance. The statistical analysis functions for the ^{32}S+^{16}O mass partition are shown in Fig. 9. There is little resonance activity at the higher excitations in ^{48}Cr, there exist no systematic similarities between the cross-correlation functions of ^{32}S+^{16}O and the other two mass mass partitions, nor is there any evidence of correlated resonance structures at the energies of the molecular configurations in ^{48}Cr.

The frequency distribution histograms of the statistical analysis functions are shown in Fig. 10 for these three mass partitions. Also plotted with a solid line for each distribution is the appropriate Gaussian distribution for purely statistical fluctuations. For all three mass partitions the cross-correlation frequency distribution $N(C)$ displays more incidents of large positive values than the Gaussian distribution would predict. This indicates that there exists a statistically significant excess of large positive values of the cross-correlation function. The summed deviation function frequency distributions $N(\mathscr{D})$ are more symmetric about zero, but all three have a slight excess of large positive and negative values. The fact that the summed deviation function is symmetric about zero does not rule out the existence of correlated resonance structure, as a correlated resonance is often

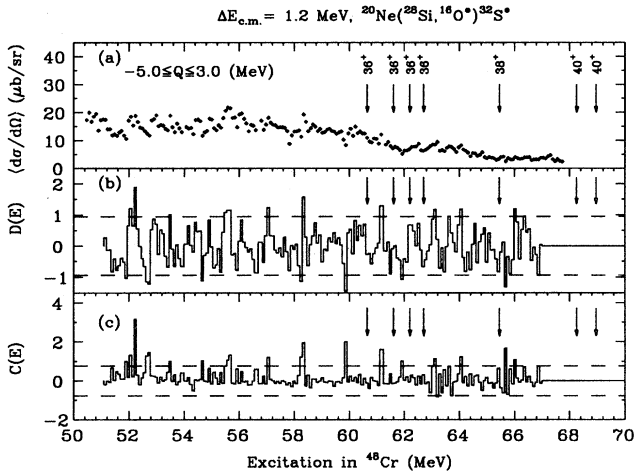

FIG. 9. (a) Sum of the excitation functions shown in Fig. 8, (b) summed deviation function, (c) cross-correlation function. The vertical arrows indicate the centroid energies for the molecular configurations [6], and the spin assignments are also listed.

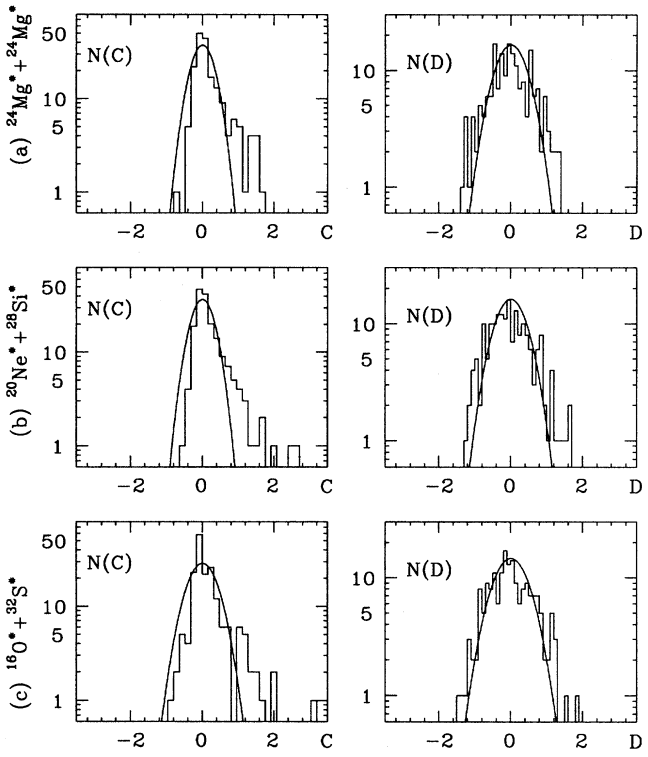

FIG. 10. Frequency distributions of the cross-correlation and summed deviation functions for the three mass partitions studied in the ^{28}Si+^{20}Ne system.

enclosed by regions of excitation energy that have negative deviation values. Therefore it is not unusual to observe comparable amounts of large positive and negative values of the deviation function for a given set of correlated resonances. The results of the frequency distributions are summarized in Table I, which also includes the expected means and standard deviations for statistical fluctuations, as well as the results from earlier studies of the ^{24}Mg(^{24}Mg,^{24}Mg*)^{24}Mg* [37] and the ^{28}Si(^{28}Si,^{28}Si*)^{28}Si* [4] reactions. The three mass partitions investigated in the current work are more similar to the ^{28}Si(^{28}Si,^{28}Si*)^{28}Si* than to the ^{24}Mg(^{24}Mg,^{24}Mg*)^{24}Mg* results. The ^{24}Mg(^{24}Mg,^{24}Mg*)^{24}Mg* cross-correlation frequency distribution has the largest variance (σ^2_{expt}) and mean (μ_{expt}), and such a large asymmetry suggests correlated resonance structure at a level much greater than could ever be randomly generated from purely statistical fluctuations in a reasonable amount of time, whereas the ^{28}Si(^{28}Si,^{28}Si*)^{28}Si* result suggests correlated structure at a level weaker than the correlations in ^{24}Mg(^{24}Mg,^{24}Mg*)^{24}Mg*, as do the results from the current work.

The structures at excitation energy=56.2 MeV are among the most strongly correlated resonances in the current work, since all three mass partitions manifest resonance phenomena at this energy. In addition, the resonance in ^{20}Ne(^{28}Si,^{24}Mg(g.s.))^{24}Mg(g.s.) at 56.2 MeV plotted in Fig. 4 has a large signal-to-background ratio, therefore an angular distribution of this reaction was measured and is shown in Fig. 11. Since the signal-to-background ratio is so large for this resonance, the resonating partial wave (assuming a single partial wave is resonating) accounts for the vast majority of the total cross section at this excitation energy, and the angular distribution is dominated by the angle dependence of this partial wave. The results of fits to single Legendre polynomials are summarized in Table II, and from these we tentatively assign a spin of $J^\pi=32^+$ to this resonance. In the following discus-

TABLE I. Summary of frequency distributions for the ^{28}Si+^{20}Ne system.

Reaction	N	Function	σ^2_{expt}	σ^2_{theor}	μ_{expt}	μ_{theor}
^{24}Mg*+^{24}Mg*	5	$C(E)$	0.1913	0.1	0.1826	0
^{24}Mg*+^{24}Mg*	5	$\mathscr{D}(E)$	0.3461	0.2	4.385×10^{-7}	0
^{28}Si*+^{20}Ne*	5	$C(E)$	0.2439	0.1	0.2067	0
^{28}Si*+^{20}Ne*	5	$\mathscr{D}(E)$	0.2060	0.2	-2.907×10^{-7}	0
^{32}S*+^{16}O*	4	$C(E)$	0.2818	$0.1\bar{6}$	0.1687	0
^{32}S*+^{16}O*	4	$\mathscr{D}(E)$	0.3765	0.25	-8.524×10^{-7}	0
^{24}Mg(^{24}Mg,^{24}Mg*)^{24}Mg*	5	$C(E)$	0.8793	0.1	0.4230	0
^{24}Mg(^{24}Mg,^{24}Mg*)^{24}Mg*	5	$\mathscr{D}(E)$	0.5386	0.2	5.897×10^{-7}	0
^{28}Si(^{28}Si,^{28}Si*)^{28}Si*	5	$C(E)$	0.470	0.1	0.027	0
^{28}Si(^{28}Si,^{28}Si*)^{28}Si*	5	$\mathscr{D}(E)$	0.429	0.2	−0.005	0

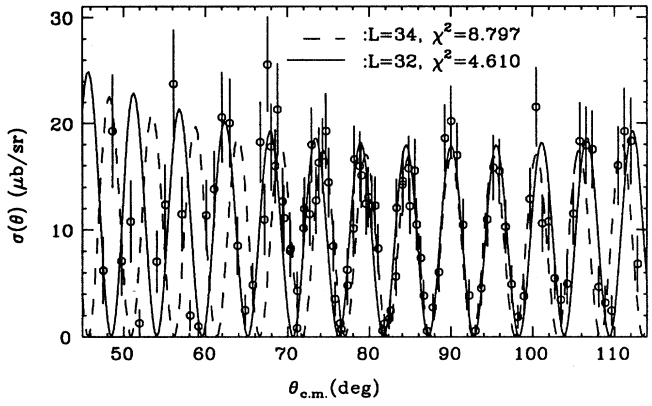

FIG. 11. Angular distribution at 56.22 MeV for the ^{20}Ne(^{28}Si, ^{24}Mg(g.s.))^{24}Mg(g.s.) reaction. Also plotted are the squares of two Legendre polynomials: $L=32$ (solid line), $L=34$ (dashed line).

sion we assume that all resonances centered at this excitation energy are dominated by $J^{\pi}=32^{+}$.

The partial widths of the various binary decay channels that manifest resonance behavior at 56.2 MeV of excitation were calculated with the Breit-Wigner formalism for the on-resonance cross section, using the assumptions that the on-resonance contribution to the cross section is added incoherently to the off-resonance cross section and is dominated by $\sigma_{\rm res}(\theta_{\rm c.m.}) \sim P_l^2[\cos(\theta_{\rm c.m.})]$. The Breit-Wigner partial widths are used to compare the measured reduced widths γ^2 with the Wigner single particle limit $\gamma_{\rm SP}^2$. For the ^{28}Si+^{20}Ne, ^{24}Mg+^{24}Mg, and ^{32}S+^{16}O channels the single particle limit is 71, 69, and 78 keV, respectively. The reduced widths for the inelastic channels were calculated assuming the stretched configuration of the spins, $l=32-S$, where $S=S_1+S_2$ is the sum of the intrinsic spins of the decay fragments. The Coulomb functions were calculated with ABACUS [43] and MATHEMATICA [44].

The so-obtained resonance parameters for the structures centered at 56.2 MeV are presented in Table III. Quite surprisingly, the branching ratio for decay into the elastic channel is equal to the branching ratio for decay to the mutual ground state of the alpha transfer channel ^{24}Mg+^{24}Mg. This is very different behavior from the molecular resonances previously studied, in which fission into the symmetric mass mutual ground state binary decay channel is at least 5 times larger than the asymmetric mutual ground state channel. The sum of the branching ratios for the $J^{\pi}=32^{+}$ resonance is comparable to the summed branching ratios in the binary fission of the previously studied molecular resonances, but is more evenly distributed between the ^{24}Mg+^{24}Mg and ^{28}Si+^{20}Ne mass partitions. The reduced width ratios $\gamma_{\alpha}^2/\gamma_{\rm SP}^2$ are larger than the reduced width ratios for the $J^{\pi}=36^{+}$ resonances [10]. There even exists evidence of decay into the highly asymmetric ^{32}S+^{16}O channel with a strength comparable to the decay of the molecular resonances into the ^{28}Si+^{20}Ne mass partition.

TABLE II. Summary of fits to the ^{20}Ne(^{28}Si,^{24}Mg)^{24}Mg angular distribution.

Excitation energy in ^{48}Cr (MeV)	Legendre polynomial	Reduced χ^2
56.22	28	44.89
56.22	30	13.72
56.22	32	4.61
56.22	34	8.80
56.22	36	14.00

Such highly fragmented decay suggests that the structure of the $J^{\pi}=32^{+}$ resonance is very different from the molecular configurations, and that the structures found in the current work are more complex and do not belong to the same rotational band as the molecular configurations. Using the spacings between the clusters of resonances in Fig. 5 as a reference, the energy region around 56 MeV would correspond to a molecular configuration with spin $J^{\pi}=34^{+}$. The spin assignment $J^{\pi}=32^{+}$ is two units lower than this value. It is tempting to speculate that the resonance manifests such fragmented decay because the spin is closer to the grazing angular momentum of all three mass partitions, and if the resonance is not strongly shape matched with a particular configuration in one of the mass partitions, then there exist several decay channels that are able to supply the large angular momentum needed for binary fission decay.

The mutual ground state exit channels for the three mass partitions studied in the current work are plotted again in Fig. 12, along with the elastic channel of the ^{24}Mg(^{24}Mg,^{24}Mg*)^{24}Mg* reaction [6]. Also plotted is the summed excitation function for the lowest two single excitations of the first 2^{+} state in the ^{28}Si+^{20}Ne inelastic channel. The $J^{\pi}=32^{+}$ spin assignment from the current work is indicated in Fig. 12(c) (all spin assignments in parentheses are based on angular distributions; those not in parentheses are from angular correlation analysis). The energy interval

TABLE III. Exit channel parameters for the resonances centered at 56.2 MeV.

Γ (keV)	Mass partition	Exit channel	$\frac{\Gamma_{\alpha}}{\Gamma}\times 10^{-2}$	$\frac{\gamma_{\alpha}^2}{\gamma_{sp}^2}\times 10^{-2}$
350±35	^{28}Si+^{20}Ne	$(0^{+},0^{+})$	1.50	2.67
350±35	^{28}Si+^{20}Ne	$(2^{+},0^{+})$	3.00	4.14
350±35	^{24}Mg+^{24}Mg	$(0^{+},0^{+})$	1.50	3.30
350±35	^{24}Mg+^{24}Mg	$(2^{+},0^{+})$	2.25	3.05
350±35	^{24}Mg+^{24}Mg	$(4^{+},2^{+})$	6.03	4.95
350±35	^{32}S+^{16}O	$(0^{+},0^{+})$	0.07	0.08
	Total	-	14.35	-

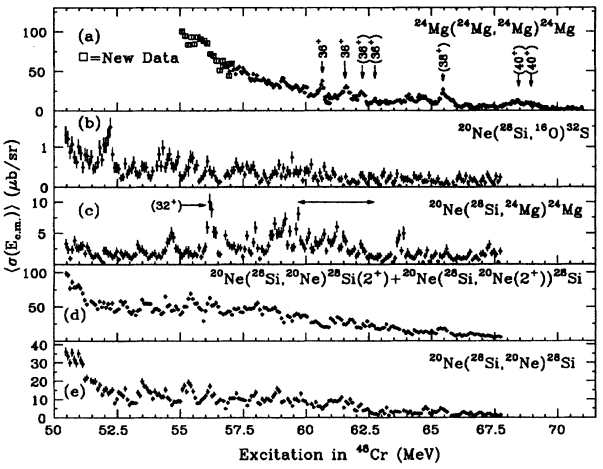

FIG. 12. A comparison of all reactions studied to date. Known spin assignments for resonances are labeled.

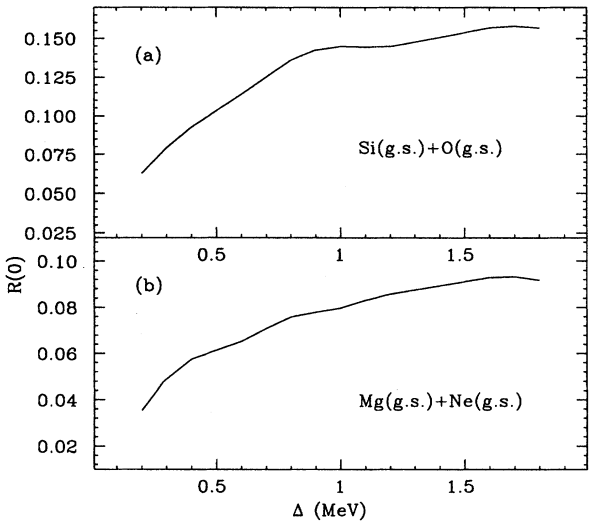

FIG. 13. Autocorrelation function for the ground-state–ground-state exit channel of each mass partition studied in the ^{24}Mg+^{20}Ne system.

marked by the horizontal arrows in Fig. 12(c) is the region studied previously [10] with the time-reversed reaction. The data in Fig. 12(a) plotted with a box symbol are previously unpublished data using a 30 μg/cm^2 ^{24}Mg target on a 15 μg/cm^2 ^{12}C backing, and a ^{24}Mg beam from the University of Pennsylvania Tandem Accelerator.

A comparison of the cross sections in the ^{24}Mg(^{24}Mg, ^{24}Mg(g.s.))^{24}Mg(g.s.), ^{20}Ne(^{28}Si, ^{24}Mg(g.s.))^{24}Mg(g.s.), and ^{20}Ne(^{28}Si, ^{20}Ne(g.s.))^{28}Si(g.s.) reactions makes it possible to determine if the few instances of concurrent resonance structure found in all three reactions is due to decay from excited states in ^{48}Cr. Using the first two reactions, the two relevant partial widths have already been calculated for some of the molecular resonances [10], and the partial widths for the ^{28}Si+^{20}Ne mutual ground state exit channel can be used to calculate the expected cross section in the ^{20}Ne(^{28}Si, ^{20}Ne(g.s.))^{28}Si(g.s.) reaction for decay from the molecular resonances. Consider the $J^\pi=36^+$ resonance centered at 62.25 MeV. For this resonance the branching ratios for the ^{24}Mg+^{24}Mg and the ^{28}Si+^{20}Ne mutual ground state channels are 1.39% and 0.19%, respectively [10], and the contribution from this resonance to the ^{28}Si+^{20}Ne elastic channel is approximately 0.4 μb/sr. The resonance contribution to the cross section in the ^{28}Si+^{20}Ne elastic channel [Fig. 12(e)] at 62.25 MeV of excitation is about 10 times larger than this value. Therefore the correlation between the ^{28}Si+^{20}Ne and ^{24}Mg+^{24}Mg elastic channels at this excitation energy is not due to decay from a molecular resonance in ^{48}Cr, and it is possible that different partial waves dominate these two elastic channels. The same conclusion holds for the other instances of concurrent correlated resonances in these three reactions.

An earlier experiment [10] concluded that the molecular configurations in ^{48}Cr did decay into the ^{28}Si+^{20}Ne mass partition. It is apparent now that the conclusion of substantial systematic molecular configuration parentage which was based on the small region of excitation energy studied was not indicative of the systematics of the two systems. As the current work illustrates, for the region of excitation energy studied previously, the agreement between Figs. 12(a) and 12(c) is reasonable. However, the correlations do not continue at the same level of significance over the entire region of excitation energy studied in the current work. The possibility that the correlations reported previously [10] are accidental cannot be ruled out.

V. RESULTS AND ANALYSIS FOR ^{24}Mg+^{20}Ne

Figure 13 plots the autocorrelation function $R(0)$ as a function of the averaging interval Δ for the mutual ground state exit channel for two mass partitions. The autocorrelation function for the ^{24}Mg+^{20}Ne mass partition is smoothly varying and reaches its plateau value gradually. The ^{28}Si+^{16}O channel has a sharper bend in its autocorrelation function, but both functions have a plateau near $\Delta=1.5$ MeV. For the ^{28}Si+^{16}O channel, any value of Δ greater than 0.9 MeV would be acceptable, but to be consistent a value of $\Delta=1.2$ MeV was used for all the statistical analysis included in the current work. As was the case with the analysis of the ^{28}Si+^{20}Ne system, the results of the statistical analysis are not very sensitive to the actual value of Δ, as long as it is near or within the plateau region. The excitation functions used for this analysis are plotted later in this section.

The excitation functions for the ^{24}Mg+^{20}Ne mass partition are shown in Fig. 14. The most pronounced structures are in the lower halves of the excitation functions; the upper halves (corresponding to excitations in ^{44}Ti greater than approximately 64 MeV) appear rather featureless. There is evidence of pronounced correlated resonant structure for the $(2^+,2^+)$, $(4^+,0^+)$, and $(4^+,2^+)$ exit channels, especially at 52.9 MeV of excitation. The widths of the structures are very characteristic of the resonance widths seen previously in this mass region.

The cross-correlation and summed deviation functions, using all possible pairs of the five excitation functions and all five excitation functions, respectively, are shown in Fig. 15. The dashed horizontal lines represent the 95% confidence

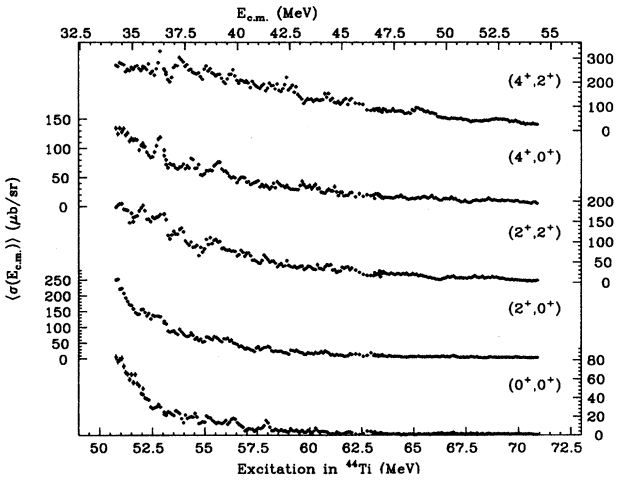

FIG. 14. Excitation functions for the ^{24}Mg+^{20}Ne mass partition. The elastic channel is averaged over the angle range 77° $\leqslant \theta_{c.m.} \leqslant$ 120°. The x axis is labeled with the excitation energy in ^{44}Ti at the bottom and with the entrance channel center of mass energy on top.

limits for statistical fluctuations. Strong correlations exist at 52.9 and 66.9 MeV, weaker ones at 53.8, 60.9, and 62.05 MeV. Using the spacings between the resonances in ^{24}Mg(^{24}Mg, ^{24}Mg*)^{24}Mg* as a reference, the spacings between the excitation energies of significant correlated resonant structure are much too large for these resonances to be attributed to consecutive spins of a molecular configuration in ^{44}Ti.

The excitation functions for the ^{28}Si+^{16}O partition are shown in Fig. 16. This mass partition has a very high density of resonance phenomena, and there exist some energies, such as at 53.2 MeV, for which the resonant structure is highly correlated between the three exit channels. Structures as narrow as those seen in ^{24}Mg(^{24}Mg, ^{24}Mg*)^{24}Mg* are observed in Fig. 16, such as at excitation energy=53.2 and 56.7 MeV.

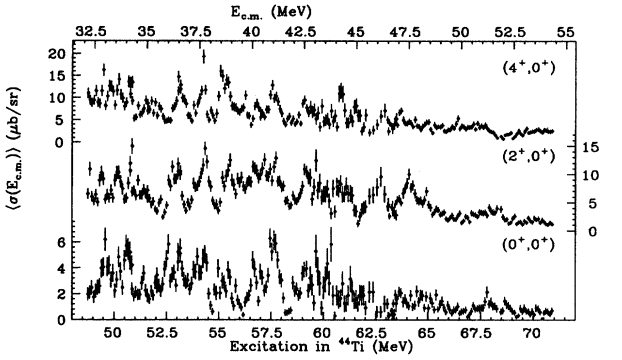

FIG. 16. Excitation functions for the ^{28}Si+^{16}O mass partition. The (0^+-0^+) channel is averaged over the angle range 49° $\leqslant \theta_{c.m.} \leqslant$ 87°. The x axis is labeled with the excitation energy in ^{44}Ti at the bottom and with the entrance channel center of mass energy on top.

At excitations in ^{44}Ti greater than approximately 66 MeV, the resonance activity becomes much less pronounced. The cross-correlation and summed deviation functions, using all possible pairs of the three excitation functions and all three excitation functions, respectively, are shown in Fig. 17. The excitation energies of correlated structure in the ^{28}Si+^{16}O and ^{24}Mg+^{20}Ne mass partitions do not coincide.

Two on-resonance angular distributions for the mutual ground state exit channel of the ^{28}Si+^{16}O mass partition for excitation energy=53.02 and 57.75 MeV are shown in Fig. 18. Based on the fits to Legendre polynomials, which are summarized in Table IV, the spin assignments are $J^\pi=25^-$ and $J^\pi=29^-$ for 53.02 and 57.75 MeV, respectively, although $l=31$ also yields a very good fit to the angular distribution at 57.75 MeV. Only odd partial waves were considered for each angular distribution. The resonance centered at 57.75 MeV is much better described by a single partial wave than is the one at 53.02, which is near another resonance centered at excitation energy=52.6 MeV, and interference

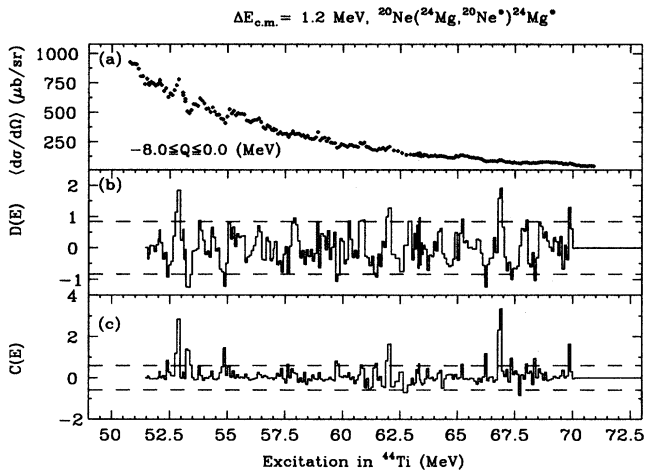

FIG. 15. (a) Sum of the excitation functions shown in Fig. 14, (b) summed deviation function, (c) cross-correlation function.

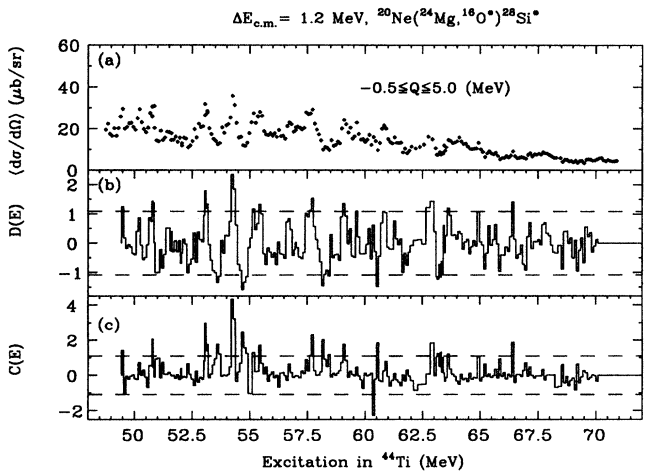

FIG. 17. (a) Sum of the excitation functions shown in Fig. 16, (b) summed deviation function, (c) cross-correlation function.

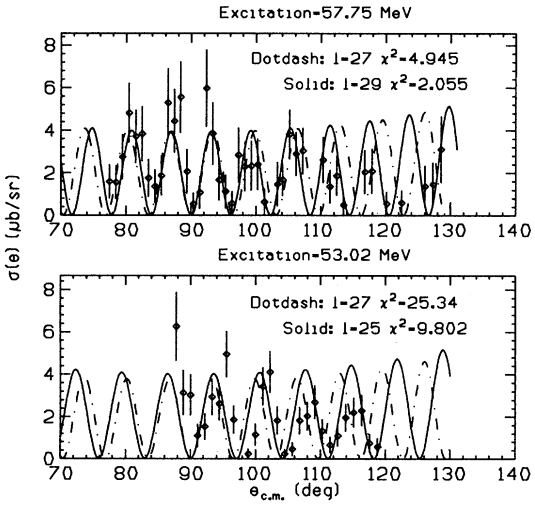

FIG. 18. Angular distributions for the $(0^+\text{-}0^+)$ channel of the $^{28}Si+^{16}O$ mass partition for two excitation energies in ^{44}Ti. The plotted curves represent squared Legendre polynomials of order labeled in the figures.

from the other peak may be complicating the behavior of the angular distribution at 53.02 MeV.

The results of optical model calculations of grazing angular momenta using the parameters listed in Table V, which are derived from fits to $^{24}Mg+^{20}Ne$ off-resonance elastic scattering angular distributions [37], are indicated in Table VI for the $^{24}Mg+^{20}Ne$ entrance channel, and for the time-reversed reaction for the $^{28}Si+^{16}O$ mutual ground state exit channel, for the excitation energies of the two on-resonance angular distributions plotted in Fig. 18. The spin assignments are roughly equal to the $^{24}Mg+^{20}Ne$ entrance channel values, and below the exit channel values. It is possible that the larger grazing angular momenta in the $^{28}Si+^{16}O$ exit channel is what makes the density of resonances so large, as there might exist many states in the $^{44}Ti \Rightarrow ^{28}Si^*+^{16}O^*$ binary fission channels that can support the entrance channel spin.

The frequency distributions of the cross-correlation and

TABLE IV. Summary of fits to the $^{28}Si+^{16}O$ angular distributions.

Excitation energy in ^{44}Ti (MeV)	Legendre polynomial	Reduced χ^2
53.02	21	27.69
53.02	23	16.05
53.02	25	9.80
53.02	27	25.34
53.02	29	33.77
57.75	23	7.38
57.75	25	5.93
57.75	27	4.94
57.75	29	2.05
57.75	31	2.58
57.75	33	13.39

TABLE V. Optical model parameters for $^{24}Mg+^{20}Ne$ elastic scattering.

V_0 (MeV)	r_0 (fm)	a (fm)	W (MeV)	r_0' (fm)	a' (fm)	r_{0C} (fm)
38.0	1.190	0.642	10.0	1.146	0.659	1.20

summed deviation functions for each mass partition are shown in Fig. 19, along with the appropriate Gaussian approximation for statistical fluctuations. Both mass partitions have a cross-correlation frequency distribution $N(C)$ with a tail that extends to large positive values. The summed deviation functions $N(\mathscr{D})$ are more symmetric about zero, but both have a slight excess of large positive and negative values. As was discussed for the $^{28}Si+^{20}Ne$ system, the fact that the summed deviation function is symmetric about zero does not rule out the existence of correlated structure. The results of the frequency distributions are summarized in Table VII, which also includes the means and standard deviations for statistical fluctuations, and the results for the $^{24}Mg(^{24}Mg, ^{24}Mg^*)^{24}Mg^*$ [37] and the $^{28}Si(^{28}Si, ^{28}Si^*)^{28}Si^*$ [4] reactions. The $^{28}Si+^{16}O$ mass partition has a variance (σ^2_{expt}) larger than that for $^{28}Si(^{28}Si, ^{28}Si^*)^{28}Si^*$, but due to the smaller number of excitation functions included in the statistical analysis of the $^{28}Si+^{16}O$ mass partition, the discrepancy between the experimental and theoretical standard deviations is not as pronounced as it is for the $^{28}Si+^{28}Si$ reaction. Therefore, although resonance phenomena are present, the results for both the $^{28}Si+^{16}O$ and $^{24}Mg+^{20}Ne$ exit channels are qualitatively more similar to the $^{28}Si+^{28}Si$ [4] and $^{28}Si+^{24}Mg$ [5] results than they are to those for $^{24}Mg+^{24}Mg$ [6].

VI. DISCUSSION OF RESULTS

Neither of the systems studied in this work manifests resonance phenomena analagous to that observed in the $^{24}Mg+^{24}Mg$ system. The following discussion will concentrate on a reevaluation of the shape matching interpretation of the molecular resonances in ^{48}Cr in light of these new experimental results, and will show that it need not be abandoned to account for the absence of similar structure in the two systems studied in this work, as well as in other systems studied in this mass region. As was discussed in the Introduction, several models have been proposed to study the properties of ^{48}Cr at high spin and high excitation energy. Here, only one of those models will be discussed in some detail: the many-particle, many-hole Hartree-Fock formalism

TABLE VI. Grazing angular momenta values for $^{24}Mg+^{20}Ne$ system.

Excitation energy in ^{44}Ti (MeV)	Resonance spin ($\hbar$)	Mass partition	l_{gr} ($\hbar$)
53.02	-	$^{24}Mg+^{20}Ne$	25
53.02	25	$^{28}Si+^{16}O$	28
57.75	-	$^{24}Mg+^{20}Ne$	28
57.75	29	$^{28}Si+^{16}O$	30

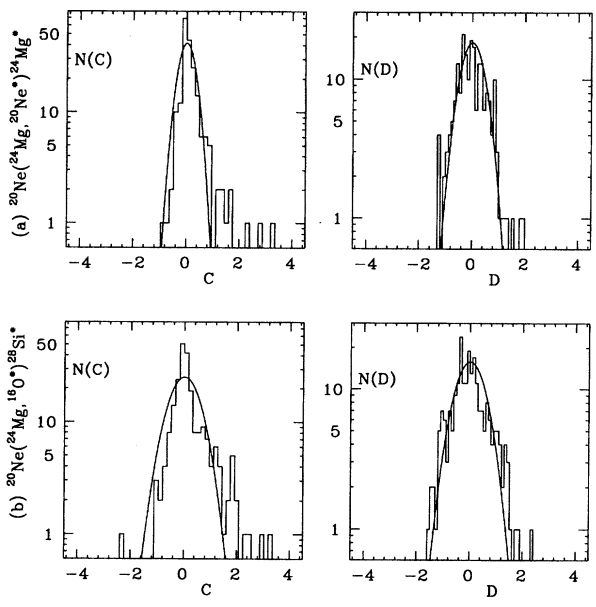

FIG. 19. Frequency distributions for the cross-correlation and summed deviation functions for the two mass partitions studied in the ^{24}Mg+^{20}Ne system.

[31]. This is the only one that considers both of the composite nuclei studied in this work, and it was also used to study the properties of ^{40}Ca, ^{52}Fe, and ^{56}Ni at large deformations. Those results are also included in this discussion. The $4m$-particle, $4n$-hole description is with respect to a spherical shell model formalism; therefore for all the Hartree-Fock (HF) excited states taken from Ref. [31], the nucleons still occupy the lowest energy single-particle states, but the nucleus is highly deformed. As a general rule the excitation energies of these Hartree-Fock excited states have an uncertainty of a few MeV, but in the following discussion a review of the Hartree-Fock calculations over a fairly large mass region will be presented, and the conclusions derived from the systematic behavior of these calculations should have just a weak dependence on the excitation energy uncertainties. In this work we follow the notation used for the Hartree-Fock calculations [31] that β_0 is the coefficient of the quadrupole term in the expansion of the shape of the nucleus. Therefore a spherical nucleus is characterized by $\beta_0=0$.

The spin versus excitation energy dependence of the resonances observed in the ^{24}Mg+^{24}Mg [6,8] and the ^{28}Si+^{28}Si systems [2] is plotted in Figs. 20 and 21, respectively. The spin versus excitation energy dependence of the grazing angular momenta for ^{24}Mg+^{24}Mg is also plotted in Fig. 20, using the parameters listed in Ref. [8]. The resonance spins for the structures observed in the ^{28}Si+^{28}Si system are consistent with the grazing angular momenta for ^{28}Si+^{28}Si, based on optical model calculations [2]. Also plotted in Figs. 20 and 21 is the spin versus excitation energy dependence of the many-particle, many-hole states in the Hartree-Fock formalism [31]. The numbers of particles and holes used for each Hartree-Fock curve are indicated. As is discussed previously and illustrated in Figs. 20 and 21, the Hartree-Fock calculations reproduce the spin versus excitation energy dependence for the resonances observed in the ^{28}Si+^{28}Si system, but not for the ones in the ^{24}Mg+^{24}Mg system.

The curves plotted in Fig. 20 suggest that the states populated in the ^{24}Mg+^{24}Mg system have a very different moment of inertia (assuming a constant moment of inertia) and a larger deformation than the $\beta_0=0.847$ that was calculated for the Hartree-Fock states. The other nuclear structure models [32–36] do not parametrize the deformation in terms of a quadrupole expansion, but a comparison [37] of the shape of a quadrupole expansion of ^{48}Cr with the calculated shape from the two-center shell model formalism [32] indicates the agreement between these two representations is reasonable for a quadrupole deformation of $\beta_0=1.3$. Therefore in this discussion the deformation of the molecular resonances in ^{48}Cr will be assigned a constant value of $\beta_0=1.3$. Perhaps the Hartree-Fock calculations would have yielded these excited states if a greater number of particle-hole excitations were considered, such as 20p-12h or 24p-16h.

The spin versus excitation energy dependence of two resonances observed in the ^{24}Mg+^{28}Si system is plotted in Fig. 22. Also plotted is the spin versus excitation energy dependence for two Hartree-Fock spin sequences calculated for ^{52}Fe. The spins of the resonances observed in the ^{24}Mg+^{28}Si system differ from the values of the grazing angular momenta [5] by only one unit of angular momenta, with one resonance having a larger spin value than the grazing angular momentum, the other a smaller spin value. Neither Hartree-Fock band reproduces the slope of the line joining the data, and it is not clear that these resonances are members of a single band in ^{52}Fe.

The predicted spin versus excitation energy dependence of the grazing angular momenta of several mass partitions

TABLE VII. Summary of frequency distributions for the ^{24}Mg+^{20}Ne system.

Reaction	N	Function	σ^2_{expt}	σ^2_{theor}	μ_{expt}	μ_{theor}
^{24}Mg*+^{20}Ne*	5	$C(E)$	0.2465	0.1	0.1506	0
^{24}Mg*+^{20}Ne*	5	$\mathscr{D}(E)$	0.3204	0.2	1.657×10^{-6}	0
^{28}Si*+^{16}O*	3	$C(E)$	0.5478	$0.\overline{3}$	0.2117	0
^{28}Si*+^{16}O*	3	$\mathscr{D}(E)$	0.4744	$0.\overline{3}$	2.492×10^{-7}	0
^{24}Mg(^{24}Mg,^{24}Mg*)^{24}Mg*	5	$C(E)$	0.8793	0.1	0.423	0
^{24}Mg(^{24}Mg,^{24}Mg*)^{24}Mg*	5	$\mathscr{D}(E)$	0.5386	0.2	5.897×10^{-7}	0
^{28}Si(^{28}Si,^{28}Si*)^{28}Si*	5	$C(E)$	0.470	0.1	0.027	0
^{28}Si(^{28}Si,^{28}Si*)^{28}Si*	5	$\mathscr{D}(E)$	0.429	0.2	-0.005	0

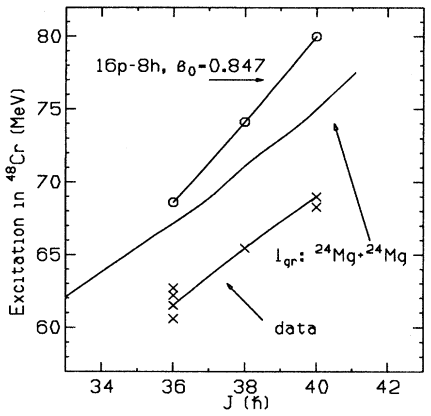

FIG. 20. The spin assignments for the resonances observed in the ^{24}Mg+^{24}Mg system are compared with the spins and excitation energies of the Hartree-Fock calculations for ^{48}Cr [31]. The quantity β_0 is the calculated quadrupole deformation of the Hartree-Fock states. Also plotted is the spin versus excitation energy dependence of the grazing angular momentum for ^{24}Mg+^{24}Mg using the parameters listed in Ref. [8].

for the ^{40}Ca [14] and ^{44}Ti composite systems is shown in Figs. 23 and 24, respectively. Also plotted in these figures is the spin versus excitation energy dependence of $l_{gr}+4$ and $l_{gr}+3$, respectively for the ^{20}Ne+^{20}Ne and ^{24}Mg+^{20}Ne entrance channels, and for the calculated many-particle, many-hole states in the Hartree-Fock formalism [31]. The grazing angular momentum values are based on optical model calculations using the parameters listed in Ref. [14] and Table V, respectively. As was discussed previously, the resonances that dominate the ^{24}Mg+^{24}Mg system have spin assignments $4\hbar$ larger than the l_{gr} of the entrance channel. The $l_{gr}+4$ and $l_{gr}+3$ curves plotted in Figs. 23 and 24, respectively, indicate that the excited states calculated in the Hartree-Fock formalism have a similar relation to the entrance channels curves as that observed between the ^{24}Mg+^{24}Mg entrance channel and

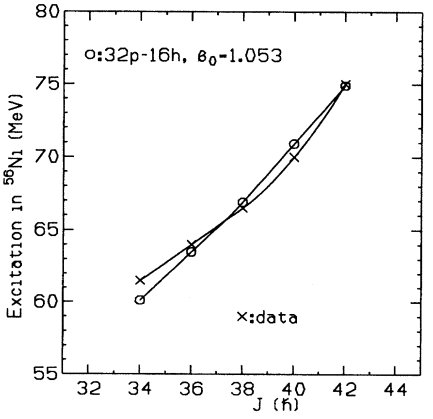

FIG. 21. The spin assignments for the resonances observed in the ^{28}Si+^{28}Si system are compared with the spins and excitation energies of the Hartree-Fock calculations for ^{56}Ni [31]. The quantity β_0 is the calculated quadrupole deformation of the Hartree-Fock states.

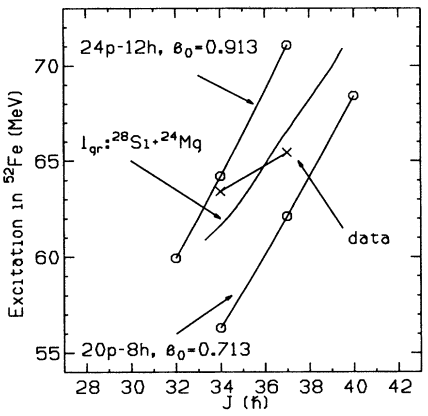

FIG. 22. The spin assignments for the resonances observed in the ^{24}Mg+^{28}Si system are compared with the spins and excitation energies of the Hartree-Fock calculations for ^{52}Fe [31]. The quantity β_0 is the calculated quadrupole deformation of the Hartree-Fock states for each rotational band. Also plotted is the grazing angular momentum versus excitation energy dependence for the ^{24}Mg+^{28}Si mass partition using the parameters listed in Ref. [5].

the molecular configurations in ^{48}Cr. However, for the ^{40}Ca and ^{44}Ti systems, the Hartree-Fock states have smaller deformations than the assumed $\beta_0 = 1.3$ of the molecular states in ^{48}Cr. This would suggest that the nuclear shapes for the excited states in ^{40}Ca and ^{44}Ti do not resemble the shape of the molecular band in ^{48}Cr, and that there is no strong shape matching between the ^{20}Ne+^{20}Ne entrance channel and the high spin states in ^{40}Ca comparable to that observed between ^{24}Mg+^{24}Mg and high spin states in ^{48}Cr. A similar conclusion is suggested for the ^{24}Mg+^{20}Ne entrance channel and the high spin excited states in ^{44}Ti.

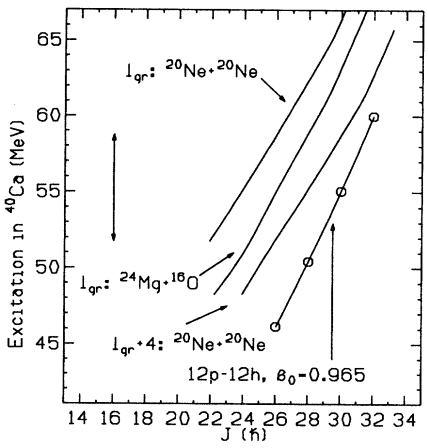

FIG. 23. The calculated curves for the grazing angular momentum versus excitation energy dependence of the ^{20}Ne+^{20}Ne and ^{24}Mg+^{16}O mass partitions are compared with the spins and excitation energies of the Hartree-Fock calculations for ^{40}Ca [31]. The quantity β_0 is the calculated quadrupole deformation of the Hartree-Fock states. The vertical arrows denote the region of excitation energy studied to date.

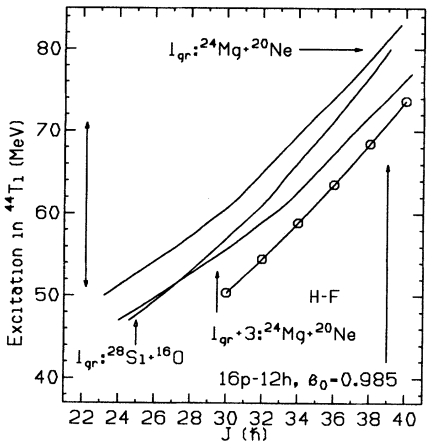

FIG. 24. The calculated curves for the grazing angular momentum versus excitation energy dependence of the ^{24}Mg+^{20}Ne and ^{28}Si+^{16}O mass partitions are compared with the spins and excitation energies of the Hartree-Fock calculations for ^{44}Ti [31]. The quantity β_0 is the calculated quadrupole deformation of the Hartree-Fock states. The vertical arrows denote the region of excitation energy studied to date.

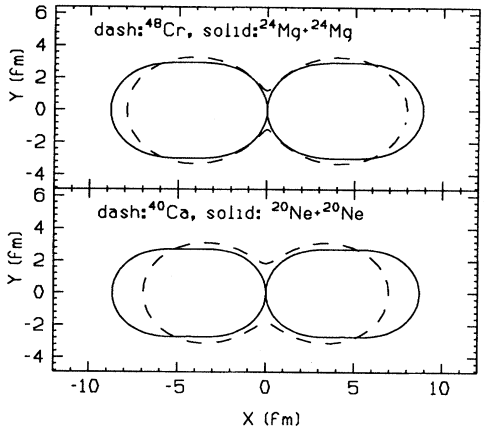

FIG. 25. The assumed surfaces of the molecular resonance excited states in ^{48}Cr and of the grazing pole-to-pole alignment of two ^{24}Mg nuclei are plotted, as are the the surfaces of the Hartree-Fock excited states in ^{40}Ca and the grazing pole-to-pole alignment of two ^{20}Ne nuclei.

The shape of the calculated Hartree-Fock states for ^{40}Ca and of the molecular states in ^{48}Cr is plotted in Fig. 25, which also plots the pole-to-pole touching configuration of the ^{20}Ne+^{20}Ne and ^{24}Mg+^{24}Mg entrance channels. The plotted shapes of the excited states are the surfaces of the nuclei in the sharp surface limit for a quadrupole expansion given by $R(\theta)=r_0[1+\beta_0 P_2(\cos\theta)]$. The deformations of ^{20}Ne and ^{24}Mg were derived from $B(E2)$ transistions [45], and are β_0 = 0.335 and 0.278 for ^{20}Ne and ^{24}Mg, respectively. In order to conserve the nuclear volume at large deformations, r_0=0.95 fm was used for ^{48}Cr and r_0=1.035 fm for ^{40}Ca, which are determined by enforcing the constraint $r_0^3[1+(3/5)\beta_0^2]=(1.2)^3$ fm^3. For both ^{20}Ne and ^{24}Mg, 1.2 fm was used for r_0. From this figure it is clear that the larger deformation of the states in ^{48}Cr greatly increases the shape matching with the ^{24}Mg+^{24}Mg system. The ground state of ^{20}Ne, has a slightly larger prolate deformation than does the ground state of ^{24}Mg, which introduces an additional shape mismatching. This shape mismatching could be the reason that correlated resonance phenomena analagous to the ^{48}Cr resonances were not observed in ^{20}Ne+^{20}Ne, ^{28}Si+^{20}Ne, and ^{24}Mg+^{20}Ne, as well as other systems. In addition, the alpha-cluster model of Rae and Merchant [34] indirectly supports this conclusion. Although neither ^{40}Ca nor ^{44}Ti has been studied with this formalism, since neither $A=40$ nor $A=44$ is "doubly magic" at the large deformations considered here, the alpha-cluster formalism suggests that neither nucleus has hyperdeformed states analagous to the predicted states in ^{48}Cr.

A more complete understanding of the resonance phenomena observed in this mass region requires more theoretical work than is reported here. The models that are currently used to study the mass-symmetric ^{24}Mg+^{24}Mg system could be used with some modification to study systems such as ^{20}Ne+^{20}Ne and ^{40}Ca, and ^{28}Si+^{28}Si and ^{56}Ni in more detail, and the mass-asymmetric systems such as ^{28}Si+^{20}Ne could be studied using the asymmetric two-center shell model formalism. In addition, the competition between resonance behavior and fusion-fission mechanisms has been studied for many composite systems in this mass region, including ^{48}Cr [46], and the results presented in this work could be useful to future studies of such competition.

ACKNOWLEDGMENTS

We would like to acknowledge the assistance of R. Antonov, F. Azfar, W. Aguirre, X. Li, D. Essiam, and G. Dorata during data acquisition. We would like to thank H. T. Fortune for helpful discussions. This work was supported by the National Science Foundation. The Wright Nuclear Structure Laboratory is supported by DOE Contract No. DE-FG02-91ER-40609.

[1] R. R. Betts, S. B. DiCenzo, and J. F. Peterson, Phys. Rev. Lett. **43**, 253 (1979).
[2] R. R. Betts, S. B. DiCenzo, and J. F. Peterson, Phys. Lett. **100B**, 117 (1981).
[3] R. R. Betts, H. G. Clerc, B. B. Back, I. Ahmad, K. L. Wolf, and B. G. Glagola, Phys. Rev. Lett. **46**, 313 (1981).
[4] S. Saini and R. R. Betts, Phys. Rev. C **29**, 1769 (1984).
[5] A. H. Wuosmaa, S. Saini, P. H. Kutt, S. F. Pate, R. W. Zurmühle, and R. R. Betts, Phys. Rev. C **36**, 1011 (1987).
[6] R. W. Zurmühle, P. Kutt, R. R. Betts, S. Saini, F. Haas, and O.

Hansen, Phys. Lett. **129B**, 384 (1983).
[7] A. Sarma and R. Singh, Z. Phys. A **329**, 195 (1988).
[8] A. H. Wuosmaa, R. W. Zurmühle, P. Kutt, S. F. Pate, S. Saini, M. L. Halbert, and D. C. Hensley, Phys. Rev. C **41**, 2666 (1990).
[9] A. H. Wuosmaa, Ph.D. thesis, University of Pennsylvania, 1988.
[10] S. Saini, R. R. Betts, R. W. Zurmühle, P. H. Kutt, and B. K. Dichter, Phys. Lett. B **185**, 316 (1987).
[11] B. K. Dichter, P. D. Parker, S. J. Sanders, R. R. Betts, and S. Saini, Phys. Rev. C **35**, 1304 (1987).
[12] R. R. Betts, in *Nuclear Physics with Heavy Ions,* edited by P. Braun-Munzinger (Harwood Academic, New York, 1984).
[13] P. H. Kutt, S. F. Pate, A. H. Wuosmaa, R. W. Zurmühle, O. Hansen, R. R. Betts, and S. Saini, Phys. Lett. **155B**, 27 (1985).
[14] S. P. Barrow, R. W. Zurmühle, J. T. Murgatroyd, N. G. Wimer, Y. Miao, K. R. Pohl, A. H. Wuosmaa, R. R. Betts, M. Freer, and B. Glagola, Phys. Rev. C **51**, 1961 (1995).
[15] C. Beck, Y. Abe, N. Aissaoui, B. Djerroud, and F. Haas, Phys. Rev. C **49**, 2618 (1994).
[16] D. A. Bromley, J. A. Kuehner, and E. A. Almqvist, Phys. Rev. **123**, 878 (1961).
[17] E. Almqvist, D. A. Bromley, J. A. Kuehner, and B. Whalen, Phys. Rev. **130**, 1140 (1963).
[18] M. L. Halbert, F. E. Durham, and A. van der Woude, Phys. Rev. **162**, 899 (1967).
[19] B. Imanishi, Nucl. Phys. **A125**, 33 (1969).
[20] Y. Kondo, Y. Abe, and T. Matsuse, Phys. Rev. C **19**, 1356 (1979).
[21] T. Matsuse, Y. Abe, and Y. Kondo, Prog. Theor. Phys. **59**, 1904 (1978).
[22] J. Y. Park, W. Greiner, and W. Scheid, Phys. Rev. C **16**, 2276 (1976).
[23] H. J. Fink, W. Scheid, and W. Greiner, Nucl. Phys. **A188**, 259 (1972).
[24] W. Scheid, W. Greiner, and R. Lemmer, Phys. Rev. Lett. **25**, 176 (1976).
[25] A. Thiel, Ph.D. thesis, Institut für Theoretische Physik der Johann-Wolfgang-Goethe Universität, 1984.
[26] K. Langanke, R. Stademann, and A. Weiguny, Phys. Lett. **112B**, 116 (1981).
[27] O. Tanimura and U. Mosel, Phys. Lett. **105B**, 334 (1981).
[28] W. A. Friedman, K. W. McVoy, and M. C. Nemes, Phys. Lett. **87B**, 179 (1979).
[29] H. Feshbach, J. Phys. Suppl. C **5**, 177 (1976).
[30] R. L. Phillips, K. A. Erb, D. A. Bromley, and J. Weneser, Phys. Rev. Lett. **42**, 566 (1979).
[31] D. C. Zheng, L. Zamick, and D. Berdichevsky, Phys. Rev. C **42**, 1004 (1990).
[32] R. Maass and W. Scheid, Phys. Lett. B **202**, 26 (1988).
[33] E. Uegaki and Y. Abe, Phys. Lett. B **231**, 28 (1989).
[34] W. D. M. Rae and A. C. Merchant, Phys. Lett. B **279**, 207 (1992).
[35] R. Maass and W. Scheid, J. Phys. G **16**, 1359 (1990).
[36] R. Maass and W. Scheid, J. Phys. G **18**, 707 (1992).
[37] S. P. Barrow, Ph.D. thesis, University of Pennsylvania, 1994.
[38] T. Ericson, Ann. Phys. (N.Y.) **23**, 390 (1963).
[39] D. M. Brink and R. O. Stephen, Phys. Lett. **5**, 77 (1963).
[40] M. G. Braga Marcazzan and L. Milazzo Colli, Prog. Nucl. Phys. **11**, 145 (1970).
[41] A. Richter, in *Nuclear Spectroscopy and Reactions*, edited by J. Cerny (Academic, New York, 1974), Pt. B, p. 343.
[42] D. Počanič, R. Čaplar, G. Vourvopoulos, and X. Aslanoglou, Nucl. Phys. **A444**, 303 (1985).
[43] S. Zawadski, computer code ABACUS (private communication).
[44] S. Wolfran, *Mathematica* (Addison-Wesley, New York, 1991).
[45] S. Raman, C. H. Malarkey, W. T. Milner, C. W. Nestor, Jr., and P. H. Stelson, At. Data Nucl. Data Tables **36**, 18 (1987).
[46] A. T. Hasan, S. J. Sanders, K. A. Farrar, F. W. Prosser, B. B. Back, R. R. Betts, M. Freer, D. J. Henderson, R. V. F. Janssens, A. H. Wuosmaa, and A. Szanto de Toledo, Phys. Rev. C **49**, 1031 (1994).